Spectroscopic Studies of Carotenoid-to-Bacteriochlorophyll Energy Transfer in LHRC Photosynthetic Complex from *Roseiflexus castenholzii*

Dariusz M. Niedzwiedzki,[†] Aaron M. Collins,[‡] Amy M. LaFountain,[§] Miriam M. Enriquez,[§] Harry A. Frank,[§] and Robert E. Blankenship*[,†,‡]

Departments of Biology and Chemistry, Washington University in St Louis, Missouri 63130 and Department of Chemistry, University of Connecticut, U-3060, 55 North Eagleville Road, Storrs, Connecticut 06269-3060

Received: January 20, 2010; Revised Manuscript Received: April 8, 2010

Carotenoids present in the photosynthetic light-harvesting reaction center (LHRC) complex from chlorosome lacking filamentous anoxygenic phototroph, *Roseiflexus castenholzii* were purified and characterized for their photochemical properties. The LHRC from anaerobically grown cells contains five different carotenoids, methoxy-keto-myxocoxanthin, γ-carotene, and its three derivatives, whereas the LHRC from aerobically grown cells contains only three carotenoid pigments with methoxy-keto-myxocoxanthin being the dominant one. The spectroscopic properties and dynamics of excited singlet states of the carotenoids were studied by steady-state absorption, fluorescence and ultrafast time-resolved optical spectroscopy in organic solvent and in the intact LHRC complex. Time-resolved transient absorption spectroscopy performed in the near-infrared (NIR) on purified carotenoids combined with steady-state absorption spectroscopy led to the precise determination of values of the energies of the $S_1(2^1A_g^-)$ excited state. Global and single wavelength fitting of the ultrafast spectral and temporal data sets of the carotenoids in solvents and in the LHRC revealed the pathways of de-excitation of the carotenoid excited states.

1. Introduction

Carotenoids (Cars) are a broad group of pigments synthesized by photosynthetic organisms that divide into two subgroups: carotenes, which are hydrocarbons, and xanthophylls, the oxygenated derivatives of carotenes. The main structural part of a Car is a long, conjugated π-electron chain of alternating carbon−carbon single and double bonds, and this is responsible for the spectroscopic properties of the molecule. The electronic absorption of Cars is typically found in the 400−550 nm spectral region and is characterized by an intense, allowed transition between the singlet electronic ground state S_0 ($1^1A_g^-$) and the second singlet excited state S_2 ($1^1B_u^+$). One photon transitions between the ground and the lowest excited electronic singlet state S_1 ($1^1A_g^-$) are forbidden by symmetry.[1−5] Carotenoids are good absorbers in the region where (bacterio)chlorophylls ((B)Chls) do not absorb well and thus, supplement the light-capturing ability of (B)Chl and facilitate the process of photosynthesis by transferring the absorbed energy to (B)Chls. Cars also play a photoprotective role by quenching (B)Chl triplet states or harmful oxygen species as they appear in antenna complexes and reaction centers (RCs). In addition, Cars have a structural role in stabilizing protein structures.

Roseiflexus castenholzii is a recently discovered thermophilic filamentous anoxygenic phototroph (FAP), able to grow photoheterotrophically in anaerobic conditions in light and in the presence of oxygen in the dark.[6] In its natural habitat, *R. castenholzii* grows symbiotically with neighboring autotrophic cyanobacteria. The photosynthetic apparatus has both similarities and differences when compared to the most well-studied FAP, *Chloroflexus aurantiacus.* It contains a reaction center (RC) with an attached *c*-type tetraheme cytochrome subunit and is in close association to a light-harvesting (LH) complex, however it lacks chlorosome antenna complexes.[6,7] The initial spectroscopic studies of the LHRC complex from *R. castenholzii* done by Collins et al.[8] revealed that the complex is spectrally similar to LH2 from purple bacteria. The major difference is the presence of the Q_y band of closely associated BChl*a* molecules at 880 nm instead of 850 nm. However, functionally this complex is more analogous to the light-harvesting I (LH1) complex from purple bacteria; and it is very probable that it surrounds the RC in the same manner as LH1. The major photosynthetic pigment is BChl*a*, however, photosynthetic membranes also contain Cars that are γ-carotene derivatives.[9] Although Takaichi et al. have investigated the Car content in whole cell extracts of *R. castenholzii*,[9] essentially no work has been done to investigate which γ-carotene derivatives are bound to the LHRC complex and what role they play in the photochemistry of the system. This work presents steady-state and ultrafast spectroscopic studies on Cars purified from the LHRC obtained from cells grown both anaerobically and aerobically. The overall objective of the work is to examine the light-harvesting function of the Cars in the LHRC complex.

2. Materials and Methods

2.1. Cell Growth. *Roseiflexus castenholzii* strain HLO8^T was grown under aerobic and anaerobic conditions described below. Both cultures were grown on 02YE media as previously described.[6] For cells grown aerobically, a 500 mL portion of a liquid culture of *R. castenholzii* was used to inoculate 8 L of 02YE media in a 22 L carboy which was closed with a foam stopper. The culture was placed in the dark, in a 50 °C incubator and stirred rapidly with a stir bar.

* To whom correspondence should be addressed. Laboratory Sciences 401B, Department of Chemistry, Washington University, St. Louis, MO 63130-4899, United States of America. Tel.: +1 314 935 7971; Fax: +1 314 935 5125.

[†] Department of Biology, Washington University in St Louis.

[‡] Department of Chemistry, Washington University in St Louis.

[§] Department of Chemistry, University of Connecticut.

10.1021/jp1005764
Published on Web 06/14/2010

For cells grown anaerobically, a 1 L culture of cells were used to inoculate 14 L of 02YE media in a 15 L fermentor (Bioengineering, Wald, Switzerland) that was surrounded with 12, 75W incandescent light bulbs. For both culture conditions, cells were harvested after 7 days of growth when they were in the stationary stage of growth.

2.2. Preparation of the LHRC. Whole membranes ($OD_{880\ nm} = 10$) in 20 mM Tris buffer (pH = 8.0) were mixed with *n*-dodecyl-β-D-maltopyranoside (DDM) to a final concentration of 0.5% for 1 h at 4 °C. The mixture was then centrifuged at 250 000 × *g* for 1 h to remove unsolubilized material. Four mL of each the solubilized anaerobic and aerobic grown membranes were loaded onto a 20−40% sucrose gradient containing 0.3% DDM and 20 mM Tris buffer (pH = 8.0). Regardless of culturing condition, the LHRC banded at approximately 33% sucrose. The LHRCs were further purified by a combination of gel filtration and ion-exchange chromatography as previously described.[8]

2.3. Pigment Extraction and Separation. Pigments were extracted by diluting concentrated LHRC complexes in a 7:2 (v/v) acetone:methanol mixture, followed by ultrasonication and centrifugation. This procedure was repeated until the resulting pellet was colorless. The mixture of pigments were dried under the steam of nitrogen and redissolved in acetonitrile:methanol: tetrahydrofuran (ACN:MeOH:THF) (58:35:7, v/v/v) and injected to an Agilent 1100 HPLC system. Pigment separation was performed with a Zorbax Eclipse XDB-C18 reverse phase column (250 mm × 4.6 mm) with an isocratic flow rate of 1.5 mL/min and ACN:MeOH:THF (58:35:7, v/v/v) mobile phase.[10] The pigments were collected, dried under a stream of argon in darkness and stored at −20 °C until further use. Carotenoids were purified with and without saponification for comparison purposes. Presence of keto-carotenoids was tested by $NaBH_4$ reduction as previously described.[11]

2.4. Mass Spectroscopy. For mass spectrometry (MS), the purified pigments were dissolved in methanol and injected using an infusion pump into an Applied Biosystems QTRAP 4000 mass spectrometer running Applied Biosystems Analyst software (version 1.4.2). The instrument used atmospheric pressure chemical ionization (APCI) in negative mode with the following parameters: curtain gas, 10 psi; collision gas, low; nebulizer current, 2.0 μA; probe temperature, 350 °C; ion source gas, 30 psi; declustering potential 130 V; and collision energy 10 eV.

2.5. Steady-State Absorption and Fluorescence Spectroscopy. Steady-state absorption spectra were recorded using a Perkin-Elmer Lambda 950 UV−vis−NIR spectrophotometer. Fluorescence and fluorescence excitation spectra were recorded using a Photon Technology International fluorometer. The fluorescence was monitored at a right-angle relative to the excitation. Excitation and emission monochromator slits were set to a bandpass of 8 nm. All fluorescence spectra were corrected for the instrument response profiles using correction factor generated using standard lamp. Fluorescence excitation spectra were corrected using a calibrated reference diode. All spectra were measured in *n*-hexane at room temperature. The integrity of the samples was checked by taking steady-state absorption spectra before and after every experiment.

2.6. Transient Absorption Spectroscopy. Transient pump−probe absorption experiments were carried out using Helios, a femtosecond transient absorption spectrometer (Ultrafast Systems, LCC), coupled to a femtosecond laser system previously described.[12] The system is based on a Spitfire-50 fs, Ti:sapphire amplifier with pulse stretcher and compressor (Spectra-Physics) pumped at 1 kHz repetition rate by Evolution 15, Q-switched Nd:YLF laser (Coherent) and seeded by pulses from Tsunami, mode-locked Ti:sapphire oscillator (Spectra-Physics), that is pumped by Millenia VsJ, diode-pumped Nd:YVO_4 CW visible laser (Spectra Physics). Output pulses, with center wavelength of 800 nm, energy of 600 mJ/pulse, ∼50 fs duration, and 1 kHz repetition were split to two beams by a beamspliter. Ninety percent of the signal was sent to OPA-800C, optical parametric amplifier (Spectra-Physics) to generate the pump beam. The remaining 10% was used to derive probe pulses. A white light continuum probe 450−800 nm in the visible region (VIS), and 800−1450 nm in the near-infrared (NIR) was generated by a 3-mm Sapphire plate. A charge-coupled detector S2000 with a 2048-pixel array from Ocean Optics was used as a detector in the VIS range. In the NIR, a 512-pixel array SU-LDV high resolution InGaAs Digital Line Camera from Sensors Unlimited was used. The pump and probe beams were overlapped at the sample at the magic-angle (54.7°) polarization. The signals were averaged over 5 s. The samples were pumped into the 0−0 vibronic band of the $S_0(1^1A_g^-) \rightarrow S_2(1^1B_u^+)$ steady-state absorption spectrum. All studies were performed at room temperature in *n*-hexane (polarity $P(\varepsilon) = 0.229$) and for keto-cars also in methanol ($P(\varepsilon) = 0.913$). The energy of the pump beam was set to 1 μJ/pulse in a spot size of 1 mm diameter corresponding to intensity between 3.0 and 3.3 × 10^{14} photons/cm^2 per pulse (depending on excitation wavelength). The optical densities (OD) of the samples were adjusted to 2.0−2.5 at the excitation wavelength in a 1 cm cuvette however, measurements were performed in 2 mm path length cuvettes. The samples were mixed continuously using a magnetic microstirrer to prevent photodegradation. The integrity of the samples was checked by taking steady-state absorption spectra before and after every experiment.

2.7. Transient Absorption Data Analysis and Fitting. Group velocity dispersion (GVD) of the transient absorption spectra was corrected using Surface Explorer (v.1.0.6) software (Ultrafast Systems LCC) by building a dispersion correction curve from a set of initial times of transient signals obtained from single wavelength fits of representative kinetics from a pure solvent sample. The number of principal kinetic components in the data sets was determined by singular value decomposition (SVD) using the same software. Global fitting analysis of the transient absorption data sets was performed using ASUfit 3.0, program provided by Dr. Evaldas Katilius at Arizona State University, with local modifications. The full width at half-maximum (fwhm) of a temporal response function of the instrument was obtained as a parameter in the global fitting analysis (Table 1).

3. Results and Discussion

3.1. Steady-State Absorption of LHRC Complexes. The absorption spectra of the LHRC complexes obtained from cells grown in aerobic and anaerobic conditions are shown in Figure 1. Differences in the Car band between 450 and 580 nm are clearly visible. With the assumption that extinction coefficients are very similar for all Cars in this protein, the aerobic sample contains around 3× more Cars. The spectral shift of the Car band maximum from 481 for the anaerobic system to 490 nm for the aerobic system suggests either that the complexes have a different Car composition or that different Cars are incorporated into each complex.

3.2. HPLC, Steady-State Absorption and Emission of Cars. Identification of the Cars bound to the LHRC was achieved using HPLC, mass spectroscopy, and chemical analysis. The HPLC chromatogram of the crude pigment extract from the LHRC of anaerobically grown cells is shown in Figure S1A

TABLE 1: Lifetimes of the $S_1(2^1A_g^-)$, Vibrational "Hot" $S_1(2^1A_g^-)$, and $S_2(1^1B_u^+)$ Excited States of γ-Carotene, Methoxy-γ-Carotene, Hydroxy-γ-Carotene, Keto-γ-Carotene and Methoxy-Keto-Myxocoxanthin

carotenoid	pump λ (nm)	τ_1 (ps)	τ'_1 (fs)	τ_2 (fs)	τ_s[a] (fs)	range	ref.
γ-carotene	490	6.0	460	130	110	VIS	this work
	490	6.0	n.e.[b]	<190	190	NIR	this work
	480	5.1	n.d.[c]	120	n.d	VIS	45
methoxy-γ-carotene	490	6.1	450	140	110	VIS	this work
	490	6.0	n.e	<190	190	NIR	this work
hydroxy-γ-carotene	490	6.2	440	140	110	VIS	this work
	490	5.6	n.e	<190	190	NIR	this work
keto-γ-carotene	495	4.4	390	110	110	VIS	this work
	495	3.8	n.e.	<190	190	NIR	this work
methoxy-keto-myxocoxanthin	505	2.5	280	<110	110	VIS	this work
	505	2.4	n.e.	<190	190	NIR	this work

[a] The fwhm of instrument response function determined by global fitting. [b] Not evident. [c] Not determined.

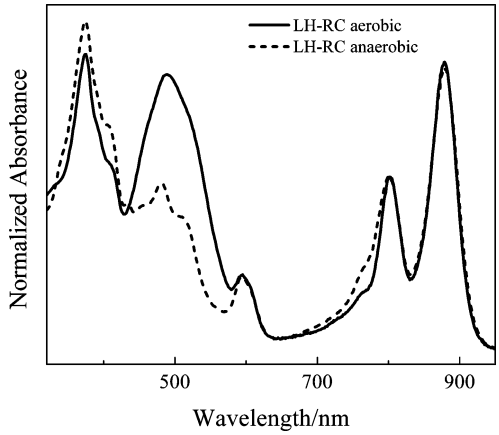

Figure 1. Steady-state absorption spectra of LHRC complex from *Roseiflexus castenholzii* grown in aerobic (solid line) and anaerobic (dashed line) conditions.

of the Supporting Information and reveals a complex pigment composition compared to the simple spectral profile of the Car absorption band of the anaerobic LHRC. There are six major, spectrally different peaks, accompanied by a few minor, unnumbered peaks, spectrally identical to the first major peak. This implies the existence of esterified derivatives for this particular Car, which was initially observed by Takaichi et al.[9] Attachment of different length esters will affect elution times of the Cars and give rise to spectrally identical peaks in a chromatogram. In order to determine if this was the case, the crude Cars extract (in 100 mL of methanol) was saponified using ~5% (w/v) KOH and then partitioned with an equal volume of *n*-hexane. Partitioning was carried out by washing the mixture with water. The top *n*-hexane layer containing the Cars was dried under a stream of nitrogen, redissolved in methanol, and injected into the HPLC system. The resulting HPLC trace is given in Figure S1C of the SI. The chromatogram still shows six distinct chromatographic peaks; however, some of the small peaks purported to be associated with Car esters are absent.

The Car composition in the aerobically grown LHRC is substantially different. The HPLC chromatogram of this sample (Figure S1B of the SI) shows only three peaks with the first one being dominant. These peaks are also present in the anaerobically grown LHRC as minor peaks. Peaks 4, 5, and 6 in Figure S1C of the SI are nearly spectrally identical having pronounced vibronic bands at 490 and 459 nm in *n*-hexane. Their elution times did not change upon saponification. This indicates that despite possessing the same chromophore, the molecules have different polarities. Peaks 1, 2, and 3 (Figures S1A, D of the SI) are not well resolved spectrally. In addition, they are shifted to longer wavelength by 3 to 10 nm compared to the spectra of peaks 4−6 (in *n*-hexane).

The spectral shift of ~10 nm may be attributed to the extension of the conjugated chain length (*N*) by one double bond. The effect of spectral broadening can be related to the presence of a keto group in the conjugated π-electron system. The presence of a keto group in the Cars isolated from HPLC peaks 1, 2, and 3 was tested by subjecting the molecules to reduction by sodium borohydride, $NaBH_4$. If a keto group is present, then it will be reduced to a hydroxyl group, which increases the polarity of the molecule, decreases its retention time, and reveals vibronic resolution typically absent when a keto group is a part of the conjugation. Figure S2 of the SI shows the HPLC results obtained from the aerobic LHRC pigment extract after being subjected to borohydride reduction. A decrease in the retention time and an increase of spectral resolution are observed and confirm the presence of a keto group in conjugation. In addition, the absorption spectrum of peak 2 contains a large "cis-peak" at ~360 nm. This indicates that it may be a central-cis isomer of the Car eluting in peak 1.

Previous studies of Cars from *R. castenholzii* performed by Takaichi et al.[9] on whole cells demonstrated that this organism contains a wide variety of γ-carotene derivatives. From a combination of results from HPLC, spectroscopy, MS, and the literature,[9] the molecular structures of the Cars bound in the LHRCs can be assigned as follows: 1′-methoxy-4-keto-myxocoxanthin (all-*trans*-peak 1 and central-*cis*-peak 2, $M = 580.43$), 4-keto-γ-carotene (peak 3, $M = 550.42$), 1′-hydroxy-γ-carotene (peak 4, $M = 554.45$), 1′-methoxy-γ-carotene (peak 5, $M = 568.46$) and γ-carotene (peak 6, $M = 536.44$). The mass spectrometry results of individual chromatographic peaks accompanied by computed mass values (M_{exp}) are shown in Figure S3 of the SI. The structures are given in Figure 2 along with the *N* values. The majority of the indentified Cars, 1′-methoxy-4-keto-myxocoxanthin, 4-keto-γ-carotene, and γ-carotene have been previously found in *R. castenholzii* cells by Takaichi and co-workers, who have also elucidated the carotenoid biosynthetic pathways in that system.[9] For convenience, simplified Car names (without numbers) will be used from here on. The HPLC results of anaerobic LHRC also reveal a short wavelength-absorbing Car present in the extract. However, it is not observed in the HPLC trace monitored at 490 nm. The 0−0 vibronic band appears at 422 nm, suggestive of an $N = 7$-like conjugated system. The pigment is most likely a Car synthesis precursor, though it is not present in the aerobic LHRC.

The steady-state absorption spectra of the identified Cars taken in *n*-hexane are given in Figures 3A−E. The spectra are associated with the electronic $S_0(1^1A_g^-) \rightarrow S_2(1^1B_u^+)$ transition

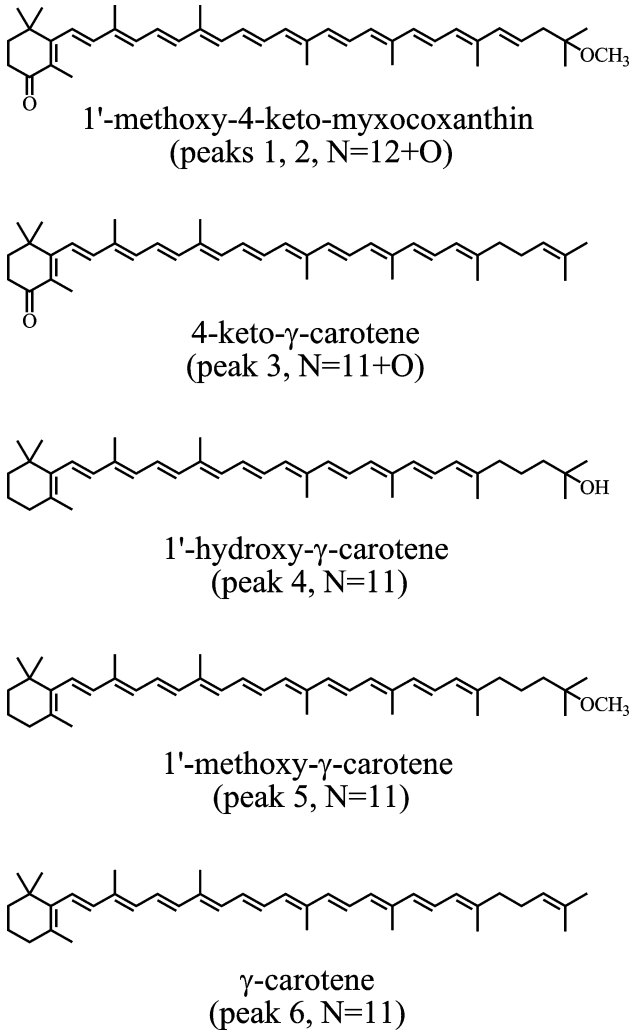

Figure 2. Structures of all-*trans* isomers of 1′-methoxy-keto-myxocoxanthin, 4-keto-γ-carotene, 1′-hydroxy-γ-carotene, 1′-methoxy-γ-carotene, and γ-carotene. The structures are given according to chromatographic peak order. Number of conjugated carbon−carbon double bounds (*N*) is also shown.

and are presented according to increasing *N*: from γ-carotene (Figure 3A) with $N = 11$ to methoxy-keto-myxocoxanthin (Figure 3E) with $N = 12+O$, where "+O" indicates that conjugation is extended to a carbonyl group. The absorption spectra shift to longer wavelengths with increasing *N*. Also, the diminishing of vibronic resolution due to the presence of a carbonyl group is evident. The steady-state fluorescence spectra of the Cars are also shown in Figure 3. For all of the molecules, the spectra are broad without clear vibronic resolution. Partial overlapping of the absorption and the fluorescence spectra indicates that emission occurs from the $S_2(1^1B_u^+)$ state.

3.3. Transient Absorption of Cars (VIS, NIR). The results of transient absorption (TA) of the studied Cars are shown in Figure 4. Transient absorption spectra were taken in both VIS and NIR regions and showed a number of spectral features originating from transitions from different excited states. In the VIS range, the negative part of the signal in the 450−520 nm range corresponds to a bleaching of the $S_0(1^1A_g^-) \rightarrow S_2(1^1B_u^+)$ ground state absorption spectrum. The sharp and very pronounced spectra in the 520−700 nm region with maximum at 554 nm for methoxy/hydroxy/-γ-carotene are associated with the $S_1(2^1A_g^-) \rightarrow S_n$ excited state absorption. This transition shifts to longer wavelengths (maximum at 585 nm) for keto-γ-carotene (Figure 4G) and methoxy-keto-myxocoxanthin (maximum at

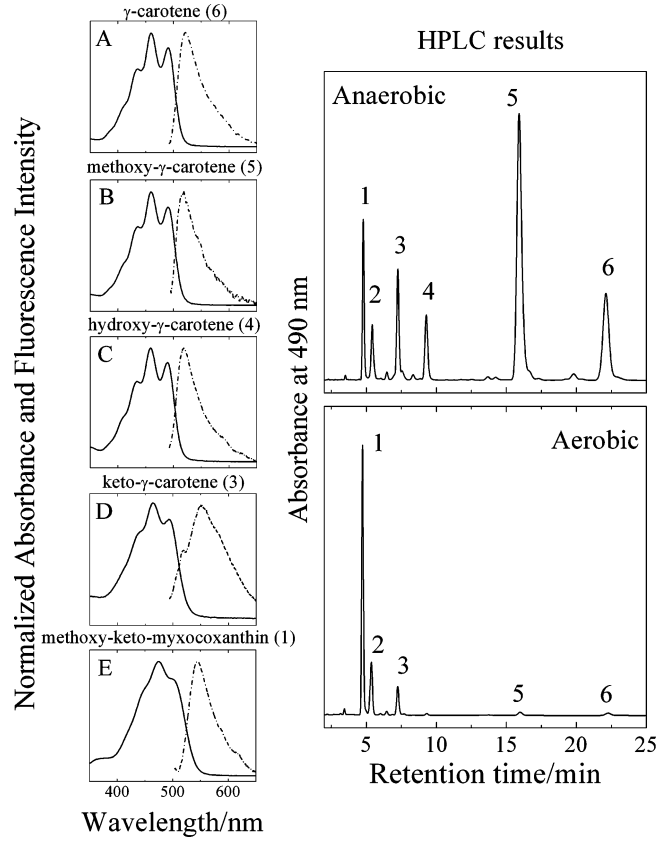

Figure 3. Steady-state absorption and fluorescence spectra of individual pigments (A−E) accompanied by HPLC chromatograms of pigment extract from LHRC complexes. The spectra are ordered according to increasing N. The numbers in parentheses indicate the peak number in the chromatograms. The spectra were taken in *n*-hexane at room temperature.

597 nm) (Figure 4I) compared to other molecules. The shift is caused by extension of the Car conjugation. A closer look at the spectra taken before 500 fs reveals broadening on the long wavelength side of the major peak. This broadening decays as time progresses and the major band narrows. The spectral broadening at this delay time scale is characteristic for vibrationally nonequilibrated transitions. In this case it is a transition from the so-called "hot" $S_1(2^1A_g^-)$ state.[12−22]

In the NIR range, two kinetically and spectrally distinguishable transitions are clearly visible. Initially, a very strong and broad band with a maximum around 1000 nm for nonketo γ-carotenes (Figure 4B,D,F), at 1100 nm for keto-carotene (Figure 4H), and at 1150 nm for methoxy-keto-myxocoxanthin (Figure 4J) decays after ~300 fs to form a weaker band that resolves into a vibronic three-peak structure. The similarity of that band to the ground state absorption spectrum suggests that it is associated with the $S_1(2^1A_g^-) \rightarrow S_2(1^1B_u^+)$ excited state absorption.

Previous studies of transient absorption of β-carotene in chloroform in the NIR region performed by Zhang et al.[24] resolved also transient signals from the radical-cation state ($D_0^{+\bullet}$) of β-carotene that appear very weakly in the 10−100 ps time domain and in the 920−960 nm spectral region. These authors have reported that radical-cation formation is caused by photooxidation of Car in the $S_2(1^1B_u^+)$ state and is solvent dependent. The signals appear in chloroform but not in hexane. The transient absorption spectra of Cars in the present study which were carried out using *n*-hexane as a solvent did not show any evidence of radical-cation transient absorption bands in the NIR as might be expected due to the solvent choice.

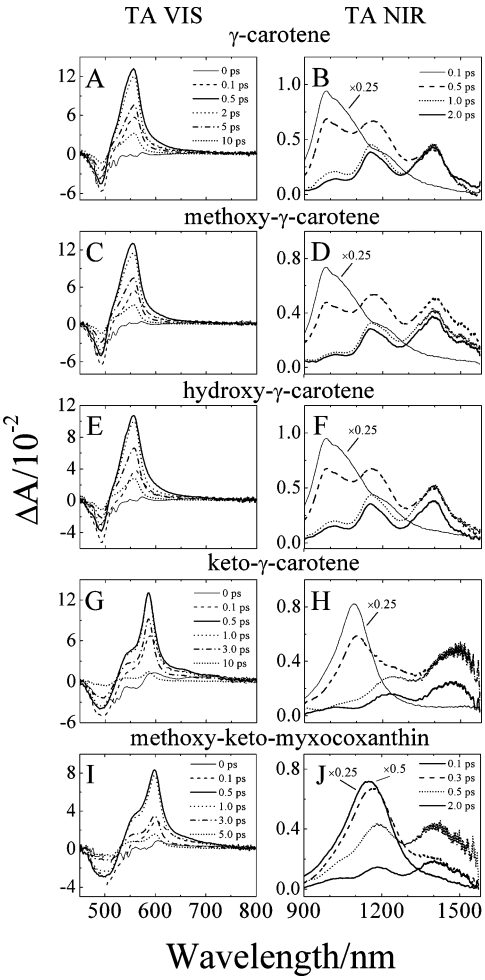

Figure 4. Transient absorption (TA) in VIS and NIR ranges for (A, B) γ-carotene, (C, D) methoxy-γ-carotene, (E, F) hydroxy-γ-carotene, (G, H) keto-γ-carotene, and (I, J) methoxy-keto-myxocoxanthin. In the NIR range early delay TA spectra were scaled to match others. The spectra were taken in *n*-hexane at room temperature.

3.4. Transient Absorption of LHRC (VIS, NIR). Transient absorption spectra of anaerobic and aerobic LHRC in the VIS (450−750 nm) and NIR (850−1350 nm) ranges taken at various delay times after Car band excitation are shown in Figure 5. Transient absorption measurements were performed for LHRC with RCs in the closed-state (no reductive agent added). The transient absorption spectra of the anaerobic LHRC in VIS range (Figure 5A) (upon excitation at 510 nm) show negative spectral features associated with bleaching of the Car ground state spectrum and two distinct positive bands with maxima at 580 and 631 nm, with the pronounced dip between them at 602 nm. The TA band is very broad and is unusual for a signal coming from a single molecule, suggesting that it originates from two different Cars. Transient absorption spectra of the anaerobic LHRC in NIR range (Figure 5B) are dominated by a strong negative band that shifts from 886 nm at early delay times to 893 nm after tens of picoseconds. This feature is a combination of bleaching of the BChl*a* Q_y band (880 nm) and stimulated emission. The weak positive signal between 950 and 1350 nm disappearing in few hundred femtoseconds is attributed to $S_2(1^1B_u^+) \rightarrow S_n$ Car transition.[24,25] Transient absorption spectra of aerobic LHRC in the VIS range (450−750 nm) (Figure 5C) reveal only one positive band. The maximum of this transition shifts to shorter wavelengths from 636 to 631 nm as delay time is increased, showing the vibrational relaxation of the $S_1(2^1A_g^-)$ state. In both samples, a long-lived shoulder at the short wavelength side of the main TA band is also visible. The spectra of the aerobic LHRC in the NIR have one notable difference compared to the anaerobic sample. The peak associated with the $S_2(1^1B_u^+) \rightarrow S_n$ transition is very pronounced and centered at 1180 nm. Similarly to the anaerobic sample, this transition disappears in few hundred femtoseconds, in a time scale typical for the Car $S_2(1^1B_u^+)$ state.[13,15]

3.5. Reconstruction of Steady-State Absorption Spectrum of LH. Detailed information about the spectral properties of the molecules contributing to the Car absorption band of the LHRC complexes provides an opportunity to reconstruct the absorption spectrum profiles. First, the absorption spectrum of the purified reaction center (RC) was subtracted from the LHRC profiles. The steady-state absorption of the RC does not show any traces of Cars and contributes additional background to the LH spectral profiles that may interfere with the accuracy of the fitting results. The amplitudes of the subtracted RC profile were adjusted to give the smallest contribution of the cytochrome Soret band at ∼415 nm. The final RC-free absorption spectra of LH complexes are shown in Figure S4 of the SI. Subsequently, the LH-only absorption spectra were converted to a wavenumber scale and a fitting procedure was applied (see below).

The HPLC results demonstrated that in the case of the anaerobic LH, seven different absorption spectra contribute to the Car band. The high spectral complexity makes the fitting procedure complicated, so to simplify it, the following assumptions were made: (1) upon binding of γ-carotene and its methoxy and hydroxy derivatives to the LH complex, these molecules will all show very similar spectra due to their comparable structures and the similarity of their spectroscopic properties in various solvents. Therefore, they all will be represented by a single spectral profile; (2) spectral shapes of the absorption bands of keto-γ-carotene and methoxy-keto-myxocoxanthin can be distorted upon binding into the protein, due to change of polarity of molecular environment. This effect is well-known for Cars with a carbonyl group closely attached to the π-electron system.[26,27] The protein environment and the water-based buffer are vastly different compared to *n*-hexane in terms of polarity. Therefore, in the reconstruction, the absorption spectra taken in the polar solvent methanol were used; (3) the absorption spectra of keto-γ-carotene and central-*cis*-methoxy-keto-myxocoxanthin are spectrally indistinguishable (except in the "cis-peak" range, see Figure S2 of the SI), and therefore will be represented as one spectral profile; (4) the relative ratio of the spectral amplitudes of the Cars bound to the LH are assumed to be indicated by the ratio of the areas of the HPLC peaks in the chromatograms. With these assumptions applied, the results of the spectral reconstruction are shown in Figure 6. The fitting procedure, written using Origin 8.0 software (OriginLab Corp, Northampton, MA, USA) allowed full freedom to vary the spectral amplitude as well as the position of each absorption spectrum, and to add them simultaneously. The results shown in Figure 6 represent fits with the best coincidence to the LH-only absorption spectra. Positions of the absorption spectra of each Car are listed in Table 2. The goodness of the reconstruction fits was also tested by taking a "LH-minus-sum" difference spectrum. In case of an ideal reconstruction, the difference spectrum should mimic the absorption spectrum of BChl *a*. These results are shown in Figure S5 of the SI and reveal very good agreement with BChl*a* bands.

3.6. Car-to-BChl*a* Energy Transfer Efficiency. The optimal detection wavelength for fluorescence excitation measurements was determined by recording emission spectra (Figure 7A). The

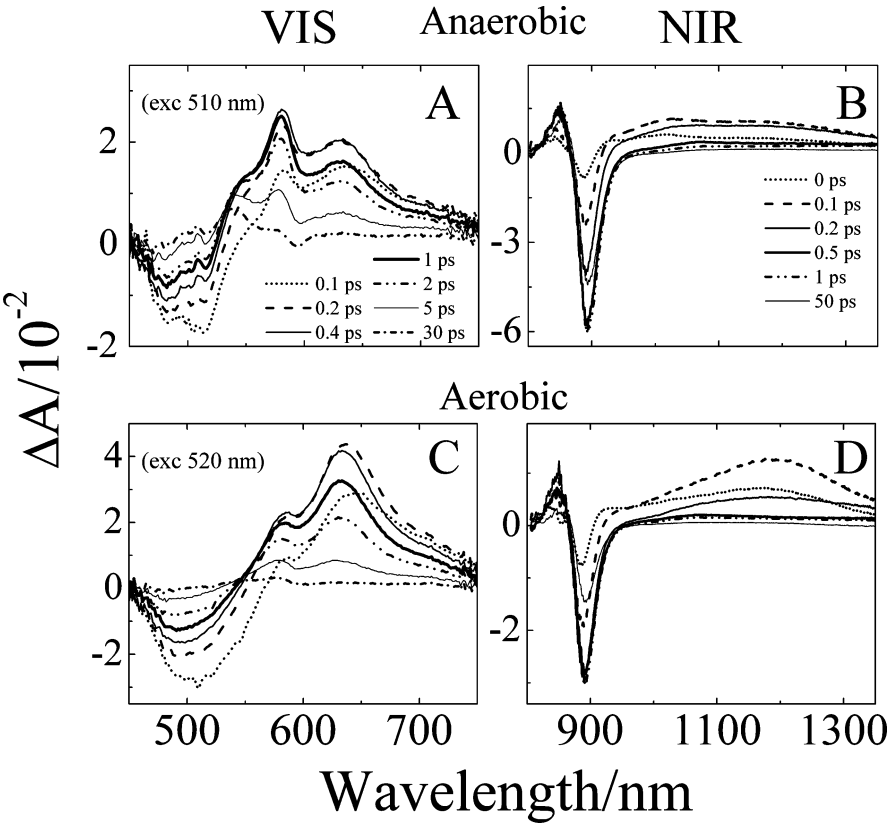

Figure 5. Transient absorption spectra of the LHRC complexes from *R. castenholzii* grown in (A, B) anaerobic and (C, D) aerobic conditions. Measurements were taken at room temperature. Samples were excited at 510 nm (anaerobic) and at 520 nm (aerobic).

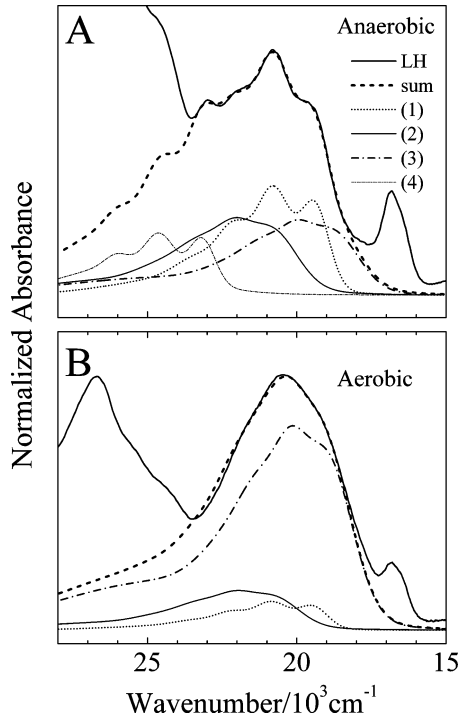

Figure 6. Reconstruction of (A) anaerobic and (B) aerobic LH-only absorption spectra. The spectral profiles associated with the individual carotenoids are as follows: (1) combined methoxy/hydroxy/-γ-carotene, (2) combined keto-γ-carotene and central-*cis*- methoxy-keto-myxocoxanthin, (3) all-*trans*- methoxy-keto-myxocoxanthin, (4) unidentified Car with short conjugation (N 7-like).

Car-to-BChl*a* excitation energy transfer (EET) efficiencies (ϕ_{ET}) were determined by taking the ratio of fluorescence excitation spectra and absorption spectra expressed as 1-*T*, where *T* is the transmittance. The spectra were normalized at BChl*a* Q_x band where was assumed that EET will be 100%. For 1-*T* profiles, LH-only absorption spectra (used for spectral reconstruction) were used. To calculate ϕ_{ET} of the most abundant Cars in the complexes: methoxy-keto-myxocoxanthin and overall ϕ_{ET} for γ-carotene and its methoxy and hydroxy derivatives, calculations were done at the specific wavelengths: 525 nm for the aerobic and 513 nm for the anaerobic LH. Reconstruction of the steady-state absorption has shown that for the aerobic LH, only methoxy-keto-myxocoxanthin contributes to overall absorption at this wavelength. For the anaerobic LH, the absorbance at 525 nm can be expressed as a linear combination of absorption of methoxy-keto-myxocoxanthin and the sum of γ-carotene and its methoxy and hydroxy derivatives. This allows a simple calculation of the unknown ϕ_{ET} of the second group of the Cars. The ϕ_{ET} efficiencies were found to be 34% for methoxy-keto-myxocoxanthin and 57% for sum of γ-carotene and its methoxy and hydroxy derivatives.

3.7. Global Fitting Results of TA of the Cars. Transient absorption data sets from Figure 4 were fit globally using an unbranched, unidirectional decay path model (A → B → C → D → ...). In this model, back-reactions are ignored on the assumption that the energy losses are large enough that the reverse reaction rates are negligible. The spectral profiles obtained from this kind of fitting of TA data sets are termed Evolution Associated Difference Spectra (EADS).[28] The fitting was done in both VIS and NIR spectral ranges and the results are shown in Figure 8. There is essentially no difference between γ-carotene (Figure 8A) and its methoxy (Figure 8C) and hydroxy (Figure 8E) derivatives. Transient absorption of these molecules taken in the VIS range was fitted by four kinetic components. The first EADS component with lifetime of 130−140 fs is associated with the $S_2(1^1B_u^+)$ state and mostly represents

TABLE 2: Energies of the $S_2(1^1B_u^+)$ and the $S_1(2^1A_g^-)$ States of the Cars and the Q_y Transitions of BChl*a* in LHRC

carotenoid	N	S_2 (cm^{-1})	S_1 (cm^{-1})	system
γ-carotene	11	20 370 ± 10	13 140 ± 60	*n*-hexane
		19 480 ± 30		LHRC (anaerobic)
		19 530 ± 30		LHRC (aerobic)
methoxy-γ-carotene	11	20 360 ± 10	13 150 ± 60	*n*-hexane
		19 480 ± 30		LHRC (anaerobic)
		19 530 ± 30		LHRC (aerobic)
hydroxy-γ-carotene	11	20 400 ± 10	13 190 ± 60	*n*-hexane
		19 480 ± 30		LHRC (anaerobic)
		19 530 ± 30		LHRC (aerobic)
keto-γ-carotene	11+O	20 190 ± 10	13 350 ± 40	*n*-hexane
		21 070 ± 50		LHRC (anaerobic)
		21 050 ± 50		LHRC (aerobic)
methoxy-keto-myxocoxanthin	12+O	19 780 ± 10	12 460 ± 40	*n*-hexane
		19 000 ± 30		LHRC (anaerobic)
		19 200 ± 30		LHRC (aerobic)
bacteriochlorophyll *a*		Q_y		
B800		12 500		LHRC (anaerobic)
B880		11 380		
B800		12 480		LHRC (aerobic)
B880		11 380		

stimulated fluorescence (negative signal) overlapping with the ground state bleaching. The second component with characteristic broad shape and lifetime of 440−460 fs is associated with the transition from the vibrationally hot $S_1(2^1A_g^-)$ state.[12−22] The third component represents TA of the fully relaxed $S_1(2^1A_g^-)$ state (lifetime of 6.0−6.2 ps). The $S_1(2^1A_g^-)$ state lifetime is known for a number of Cars with $N = 11$. It spans a wide range, from 4 to 10 ps and depends on the effective length of conjugation. Extension of the conjugation to the terminal rings of Car molecule distorts the conjugation and makes it effectively shorter. For example, lycopene ($N = 11$), a fully open chain Car with straight conjugation has $\tau_{S1} = 4$ ps while β-carotene, also with $N = 11$ but with conjugation present in two terminal rings $\tau_{S1} = 9-10$ ps.[13,29,30] The $S_1(2^1A_g^-)$ lifetimes of methoxy/hydroxy/-γ-carotene is in the midrange as can be expected for Car with $N = 11$ with conjugation extended to only one existing terminal ring. This is another verification that the structural assignment of the Cars was done correctly. There is also a long-lived EADS with 11 ps lifetime. The origin of this spectral component is unclear, but based on previous work done on Cars with long conjugation it may be associated with TA from the so-called S* state.[13,15,31] Nevertheless, the amplitude of this EADS is very small compared to other spectral features and was not further investigated here. The same number of EADS components is required to fit the TA of keto-γ-carotene (Figure 8G) and methoxy-keto-myxocoxanthin (Figure 8I). On the basis of the energy gap rule, it is known that an increase of conjugation (N) leads to a decrease of the $S_1(2^1A_g^-)$ state lifetime.[32,33] This trend is also observed here. For methoxy/hydroxy/-γ-carotene (Figure 8A, C, D) with $N = 11$ the $S_1(2^1A_g^-)$ state lifetime of ∼6 ps, shortens to 4.4 ps for keto-γ-carotene (Figure 8G, $N = 11+O$) and finally to only 2.5 ps for methoxy-keto-myxocoxanthin (Figure 8I, $N = 12+O$). The lifetimes of the EADS obtained for TA from NIR match quite well to the lifetimes of the $S_2(1^1B_u^+)$ and the $S_1(2^1A_g^-)$ states. It is clear that these transitions occur from two different excited states, $S_2(1^1B_u^+)$ and $S_1(2^1A_g^-)$, respectively. As an example of the goodness of the fitting, three kinetics with corresponding fits were extracted from VIS TA (the maximum, blue and red sides of the major TA band), and two kinetics from NIR TA (in range of TA from $S_2(1^1B_u^+)$ and from $S_1(2^1A_g^-)$ states) for each of the molecules. They are shown in Figure S6.

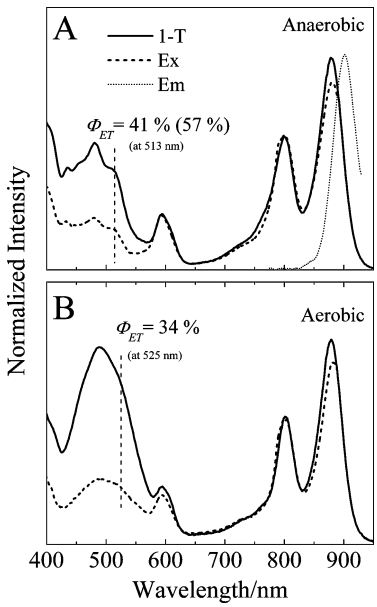

Figure 7. Fluorescence excitation (Ex), emission (Em), and 1-T (where T is transmittance) (with subtracted RC) spectra of the LH complexes in buffer at room temperature. Fluorescence excitation spectra were reordered with emission monitored at 900 nm. Value given in parentheses corresponds to the energy transfer efficiency of the collective methoxy/hydroxy/-γ-carotene group. The spectra were normalized at BChl*a* Q_x band where was assumed that EET will be 100%.

3.8. $S_1(2^1A_g^-)$ Energies. Figure 9 shows the normalized steady-state $S_0(1^1A_g^-) \rightarrow S_2(1^1B_u^+)$ absorption spectra and the $S_1(2^1A_g^-) \rightarrow S_2(1^1B_u^+)$ NIR transient absorption profiles plotted on a wavenumber scale (left column). In addition, they were also shifted to give the best agreement between the spectral traces (right column). The shift in energy required to bring the spectra into coincidence corresponds to the energy of the $S_1(2^1A_g^-)$ state of the molecules. The $S_1(2^1A_g^-)$ state energies obtained for γ-carotene (Figure 9B) and its methoxy (Figure 9D) and hydroxy (Figure 9F) derivatives ($N = 11$) are very similar, 13 140, 13 150, and 13 190 cm^{-1}, respectively. For keto-γ-carotene ($N = 11+O$) is 13 350 cm^{-1}, and 12 460 cm^{-1} for methoxy-keto-myxocoxanthin ($N = 12+O$).

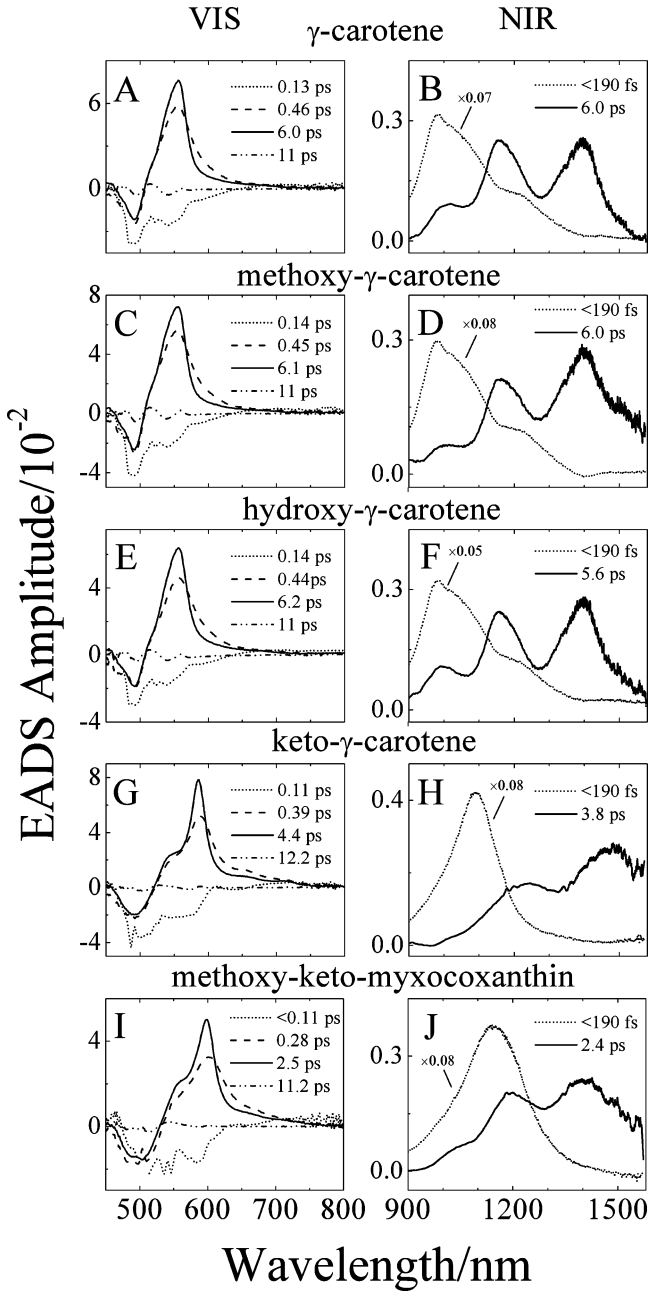

Figure 8. Global fitting results using the sequential decay model (EADS) of transient absorption data sets shown in Figure 4.

3.9. Car-to-BChl*a* Energy Transfer via $S_2(1^1B_u^+)$ and $S_1(2^1A_g^-)$ States. Cars are able to transfer energy to BChls from both $S_2(1^1B_u^+)$ and $S_1(2^1A_g^-)$ excited states. Transient absorption results of LHRC in NIR range (Figure 5B, D) show that simultaneously to decay of the $S_2(1^1B_u^+) \rightarrow S_n$ Car transition a rapid rise of BChl*a* Q_y bleaching at 880 nm is also observed, indicating ultrafast Car → BChl*a* energy transfer that occurs from the $S_2(1^1B_u^+)$ state.

Energy transfer between Car and BChl can be described by general expression for the rate constant for energy transfer between a weakly coupled donor−acceptor pair:

$$k_{ET} = \frac{1}{c\hbar}|T|^2 J \qquad (1)$$

Where T is electronic coupling term and J is the spectral overlap described by

$$J = \frac{\int_0^\infty F_d(\nu)\varepsilon_a(\nu)d\nu}{\int_0^\infty F_d(\nu)d\nu \int_0^\infty \varepsilon_a(\nu)d\nu} \qquad (2)$$

F_d is fluorescence spectrum of donor and ε_a is absorption spectrum of acceptor on a frequency mode scale. The electronic coupling term, T, has to be calculated differently for $S_2(1^1B_u^+)$ and $S_1(2^1A_g^-)$ states due to their different nature. Coupling between the $S_2(1^1B_u^+)$ state and Q_x of BChl*a* can be estimated

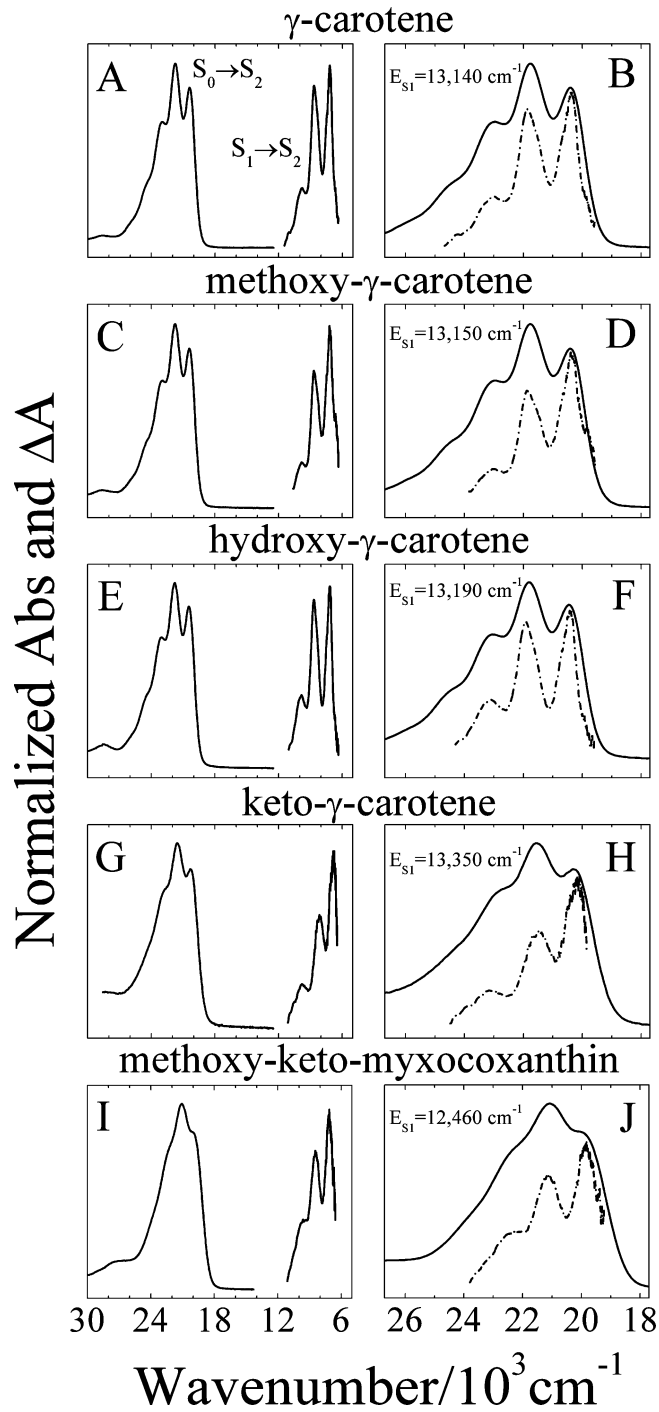

Figure 9. The $S_0(1^1A_g^-) \rightarrow S_2(1^1B_u^+)$ steady-state and the $S_1(2^1A_g^-) \rightarrow S_2(1^1B_u^+)$ transient absorption spectra presented on the wavenumber scale with corresponding overlays of both transitions giving the best peak-valley coincidence. The magnitude of the energetic shift of the $S_1(2^1A_g^-) \rightarrow S_2(1^1B_u^+)$ profile determines the $S_1(2^1A_g^-)$ state energy. The spectra were normalized to the maxima.

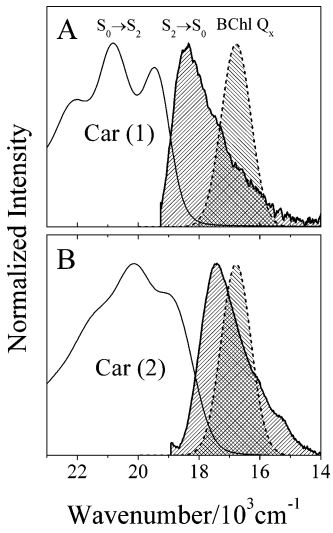

Figure 10. Spectral overlap between absorption of LHRC BChl*a* Q_x band and the $S_2(1^1B_u^+)$ fluorescence taken from (A) combined methoxy/hydroxy/-γ-carotene (Car(1)) and (B) methoxy-keto-myxocoxanthin (Car(2)) in *n*-hexane shifted to correspond to the spectral origins expected to be in the LHRC complexes.

based on Förster theory.[34] Unfortunately, the crystal structure of the LHRC complex from *R. castenholzii* is still unknown and the lack of distance information between interacting molecules and their relative orientations precludes more advanced theoretical studies. However, steady-state fluorescence spectra from the $S_2(1^1B_u^+)$ state are available (Figure 3A−E) and the spectral overlap *J* can be evaluated. Accurate estimate of the *J* value requires knowing the absorption extinction coefficient (ε) of BChl*a* Q_x band. It is not known for that complex, but relative changes of *J* for each Car can be easily obtained. The spectral overlap between absorption of BChl*a* (Q_x band of LHRC complex) and emission of the most abundant Cars (methoxy-keto-myxocoxanthin and combined methoxy/hydroxy/-γ-carotene) are given in Figure 10. The spectral overlap *J* is the largest for methoxy-keto-myxocoxanthin, almost 2× larger than for combined γ-carotene and its methoxy and hydroxy derivatives. Due to the spectral similarities of LHRC and LH2 from purple bacteria, it is probable that Cars in the LHRC will be distributed more-or-less similarly to LH2 (same distance and orientation compared to neighboring BChls), so an electronic coupling term *T* is comparable for all of the Cars. If this is true, methoxy-keto-myxocoxanthin is the best candidate for an efficient $S_2(1^1B_u^+)$ energy donor. However, these predictions do not fit to the ϕ_{ET} values obtained from fluorescence measurements and is apparent also that the $S_1(2^1A_g^-)$ state must play an important role in energy transfer control.

Figure 11 shows the $S_2(1^1B_u^+)$ and $S_1(2^1A_g^-)$ energies of studied Cars with the energies of BChl*a* Q_x and Q_y transitions in both LHRC complexes. From an energy resonance point of view the $S_1 \rightarrow Q_y$ channel is accessible for all the molecules. Theoretical calculation of the $S_1 \rightarrow Q_y$ energy transfer rate (k_{S1}) requires sophisticated techniques. Due to a negligible $S_1 \rightarrow S_0$ transition dipole moment of Car, electronic coupling *T* between Car S_1 state and BChl*a* Q_y was found by Scholes et al. to be composed of polarization and Coulombic interactions.[35] Zero transition dipole moment of $S_1 \rightarrow S_0$ makes Car fluorescence from the $S_1(2^1A_g^-)$ in practice undetectable. Lack of the true $S_1(2^1A_g^-)$ emission profile leads to a large uncertainty of the spectral overlap calculation as well. Even so, an energy transfer rate (k_{S1}) can be obtained experimentally from ultrafast time-resolved transient absorption studies of the Cars in solvents and

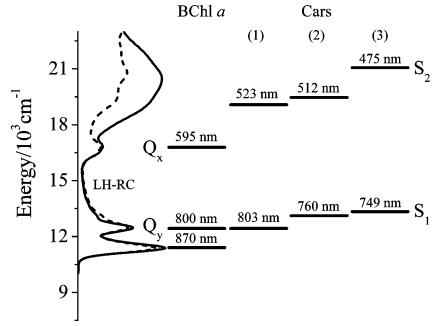

Figure 11. The $S_2(1^1B_u^+)$ and the $S_1(2^1A_g^-)$ sate energies of the Cars from the LHRC complexes of *R. castenholzii* along with energies of BChl*a* Q_x and Q_y transitions. Corresponding wavelengths are also indicated.

bound to the LH protein. In this case, depopulation of the $S_1(2^1A_g^-)$ by Car → BChl energy transfer will lead to shortening the $S_1(2^1A_g^-)$ lifetime and k_{S1} can be easily obtained from comparison of unaffected (from solvents) and affected (by energy transfer) lifetimes. Nevertheless, it is well-known that keto-Cars are able to form a charge-transfer state (ICT) in polar environments, that has significantly shorter lifetime compared to a pure $S_1(2^1A_g^-)$.[26,36,37] The present studies have shown that the best reconstruction of the LH absorption spectra is obtained if the absorption spectra of keto-Cars from methanol were used, suggesting that Cars environment (in term of polarity) in LHRC protein is similar to that solvent.

Shortening of the $S_1(2^1A_g^-)$/ICT state lifetime of Car bound to the protein with enhanced polarity can be misinterpreted as an effect of energy transfer. To preclude this possibility, TA of both keto-Cars studied here was also taken in methanol. The TA spectra along with global fitting results are shown in Figure S7 of the SI. They show some spectral broadening of TA bands but essentially no changes in excited states lifetimes are observed. This test confirms that changes in the $S_1(2^1A_g^-)$ state lifetime of keto-γ-carotene and methoxy-keto-myxocoxanthin upon binding them to LH protein will be associated mostly with Car-to-BChl energy transfer process.

Instead of global fitting analysis, a single wavelength fitting was done to obtain effective lifetimes of the $S_1(2^1A_g^-)$ of Cars bound to the LH protein. Reconstruction of the steady-state absorption spectrum of the anaerobic LH complex reveals that is impossible to excite strictly a single Car in the carotenoid band for this sample. For example, excitation at 510 nm will simultaneously excite two groups of Cars (methoxy/hydroxy/-γ-carotene and methoxy-keto-myxocoxanthin) and will result in two independent TA spectra overlapping each other. This makes extracting the effective lifetime of individual pigments difficult unless a specific wavelength with negligible TA of one of them is known. Such a point in the TA spectra of LHRC can be found by mimicking the TA profile of the LHRC complex from individual pigment spectral components.

The protein environment does not affect the energy of the Car $S_1(2^1A_g^-)$ state, although it changes (stabilizes or destabilizes) the energy of the $S_2(1^1B_u^+)$ and as well any higher B_u-like (S_n) state by a similar value. This means that the TA of the Car that is bound to the protein can be mimicked by shifting Car TA taken in organic solvent by a certain value that is equal to the shift of the steady-state absorption observed upon binding Car to the protein. The results of TA of LHRCs constructed by this way, along with the real TA of aerobic LH-RC excited at 520 nm are shown in Figure 12A. The shifted TA spectrum of methoxy-keto-myxocoxanthin (taken in methanol after 700 fs)

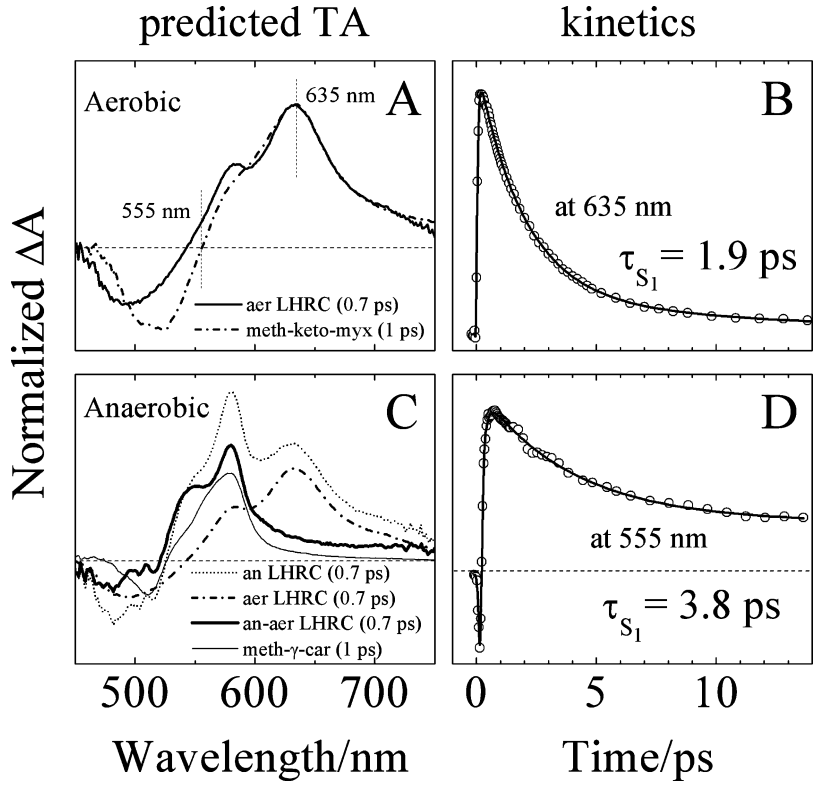

Figure 12. (A, C) TA spectra of the aerobic and anaerobic LHRC upon excitation of the Car band taken at 700 fs after excitation along with modeled spectra (see text for details). The spectra of individual pigments were taken at time delays given in parentheses; (B, D) Kinetics extracted from TA of LHRC complexes (at wavelength given in the Figure) along with corresponding fits. For clarity only the effective lifetimes of the $S_1(2^1A_g^-)$ state are given. Detailed information about fitting is given in Table S1 of the SI.

almost entirely covers the experimental profile of TA of LHRC complex. The shoulder present at the blue side of the TA spectrum originates from S* and/or triplet excited state absorption, previously observed in LH2 from purple bacteria.[18,22,25,38] Photoinduced triplet state formation for a single Car molecule dissolved in solvent is practically negligible due to extremely low quantum yield of intersystem crossing ($\sim 10^{-3}$)[39] and singlet-to-triplet fission.[40] This disadvantage makes it impossible to perform a perfect reconstruction of this spectral part of the LHRC TA profile.

On the basis of reconstruction of the Car band in the steady-state spectrum of the anaerobic LH (Figure 6), it is apparent that 510 nm excitation will stimulate TA mostly from 2 groups of Cars: combined methoxy/hydroxy/-γ-carotene and methoxy-keto-myxocoxanthin. In this case, the TA spectrum of aerobic LHRC was subtracted from the TA profile of anaerobic LHRC (Figure 12C, "an-aer LHRC"). The result should reflect the TA spectrum of LHRC in which only Cars from the methoxy/hydroxy/-γ-carotene group are present. The shape of that profile (Figure 12C, thick solid line) displays considerable similarities to typical TA of Cars in LH2.[25] There is a sharp positive band at 580 nm accompanied with a broader shoulder at the short wavelength side of the peak. According to studies done on LH2, this shoulder must be associated with TA occurring from S* and/or an excited triplet state.[18,22,25,38] In addition, the TA spectrum of methoxy-γ-carotene taken 1 ps after excitation (in *n*-hexane) is shown. Prior to overlaying, the spectrum was converted to wavenumber scale, shifted to position where bleaching of the 0−0 vibronic band of ground state absorption appeared at 19 490 cm^{-1} (513 nm), converted back to wavelength and scaled. The resulting spectrum perfectly matches the position of the experimental profile. However, this transient peak is slightly broader compared to that observable at 580 nm in the LHRC, indicating that this pigment has less conformational disorder when it is bound to the protein. Interestingly, for methoxy-keto-myxocoxanthin both profiles (in LHRC and in methanol) (Figure 12A) are broad and practically identical, demonstrating that conformational disorder induced by a carbonyl group cannot be diminished by protein environment.

The spectral profile of TA of methoxy-keto-myxocoxanthin given in Figure 12A (taken in methanol) shows that contribution from the $S_1(2^1A_g^-) \rightarrow S_n$ transition of this pigment at 555 nm in the TA of LHRC is expected to be zero and that wavelength was used to extract the effective lifetime of the $S_1(2^1A_g^-)$ state of methoxy/hydroxy/-γ-carotene. It was found to be 3.8 ps and the results are shown in Figure 12D, and also listed in detail in Table S1 of the SI. The effective lifetime of the $S_1(2^1A_g^-)$ state of methoxy-keto-myxocoxanthin was obtained from single wavelength fitting at the maximum of the TA band of the aerobic LHRC (635 nm) and is 1.9 ps (Figure 12B).

The Car-to-BChl energy transfer efficiency $\phi_{ET}(S_1)$ can be expressed as follows:

$$\phi_{ET}(S_1) = \left(1 - \frac{\tau_{S_1}^{LHRC}}{\tau_{S_1}^{SOLV}}\right) \times 100 \qquad (3)$$

where $\tau_{S_1}^{LHRC}$ and $\tau_{S_1}^{SOLV}$ are the lifetimes of the $S_1(2^1A_g^-)$ state in LHRC and in solvent, respectively. They are 37% for methoxy/hydroxy/-γ-carotene and 24% for methoxy-keto-myxocoxanthin. The same argumentation can be used to calculate $\phi_{ET}(S_2)$; however, in this case, the temporal resolution of the TA spectrometer (110 fs) limits accurate measurements. However, they can be predicted upon the assumption that the overall ϕ_{ET} obtained from steady-state fluorescence spectroscopy and

TABLE 3: Energy Flow Paths of the Major Cars Found in the LHRC Protein

	S_2	S_1	S*	ϕ_{ET}
	methoxy/hydroxy/-γ-carotene in LHRC			
τ_{eff} (k_{eff})	67 fs (14.79)[a]	3.8 ps (0.263)	~20 ps (0.08)	
branch (yield) (τ) (k)	$S_2 \rightarrow S_1$ (52%) (130 fs) (7.69)	$S_1 \rightarrow S_0$ (63%) (6.0 ps) (0.167)		
	$S_2 \rightarrow S$ (10%)$^+$ (~680 fs) (1.48)	$S_1 \rightarrow$BChl (37%) (10.4 ps) (0.096)		
	$S_2 \rightarrow$BChl (38%) (~180 fs) (5.62)			
EET (%)	38	19	0	57
	methoxy-keto-myxocoxanthin in LHRC			
τ_{eff}(k_{eff})	73 fs (13.70)[a]	1.9 ps (0.526)	~12 ps (0.08)	
branch (yield) (τ) (k)	$S_2 \rightarrow S_1$ (73%) (110 fs) (9.09)	$S_1 \rightarrow S_0$ (76%) (2.5 ps) (0.400)		
	$S_2 \rightarrow S$ (10%) (730 fs) (1.37)	$S_1 \rightarrow$BChl (24%) (8.3 ps) (0.126)		
	$S_2 \rightarrow$BChl (17%) (430 fs) (2.33)			
EET (%)	17	17	0	34

[a] Values predicted based on expression 4 (see main text).

from dynamic analysis should be equal. The total Car-to-BChl energy transfer efficiency ϕ_{ET} (in %) will be described by the following expression:

$$\phi_{ET} = \phi_{ET}(S_2) + (100 - \phi_{ET}(S_2) - \phi(S^*)) \times \frac{\phi_{ET}(S_1)}{100} \quad (4)$$

where all values are given in percent, ϕ(S*) is an efficiency of S* formation via the $S_2(1^1B_u^+)$ state. Also, it was assumed that no states other than $S_2(1^1B_u^+)$ and $S_1(2^1A_g^-)$ are included in energy transfer. The efficiency of S* formation was estimated using the same method described in detail in Cong et al.[25] and in this case is approximately 10% for the both LHRC complexes. Under such conditions, the expected $\phi_{ET}(S_2)$ are 38% for methoxy/hydroxy/-γ-carotene and 18% for methoxy-keto-myxocoxanthin. The summarized lifetimes, rates, and efficiencies are given in Table 3.

3.10. Carotenoid Radical Cation Formation. Previously, TA studies of LH2 complexes from purple bacteria *Rb. sphaeroides*[41] and most recently from *Rps. acidophila* 10050[25] performed in the NIR range revealed the presence of a transient absorption band associated with formation of the Car radical cation. This band is formed only upon excitation of Car, as demonstrated by Polivka et al.,[41] and is associated with an electron transfer process between Car and BChl*a*. It was also shown that B800 plays crucial role in the process. Upon selective perturbation of the B800 binding site in LH2 by lithium dodecyl sulfate (LDS) treatment,[42] the Car radical cation cannot be formed. Similarly, Cars reconstituted to LH2 from the *Rb. sphaeroides* R26.1 mutant that lacks the B800 band are not able to form radical cations.[41] The quantum chemical computations done by Wormit and Dreuw[43] on three Cars (neurosporene, spheroidene, and spheroidenone) employing time-dependent density functional theory in molecular model Car-BChl systems, demonstrated Car-BChl intermolecular electron transfer processes. The calculated energy level of the lowest electron transfer state (ET) of the Car-BChl heterodimer was shown to be dependent on the intermolecular distance and lay below $S_2(1^1B_u^+)$ and $S_1(2^1A_g^-)$ states for the ~3.3 Å Car-B800 distance taken from the LH2 crystal structure,[44] allowing ET formation upon direct excitation of the $S_2(1^1B_u^+)$ state. However, in the case of spheroidene, the lowest ET climbs above the $S_2(1^1B_u^+)$ state for intermolecular distance larger than 4.8 Å, precluding the possibility of radical cation formation upon Car $S_2(1^1B_u^+)$ state excitation if intermolecular distance is expanded.[43]

The LH complexes from *R. castenholzii* and LH2 from purple bacteria show large spectroscopic similarities, particularly the presence of the of B800 band. Despite this, TA of the LHRC complexes from *R. castenholzii* in the NIR range does not show any traces of Car radical cation transient absorption band.

The $S_1(2^1A_g^-)$ energies of all the Cars found in LHRC lay between 12 460 and 13 140 cm^{-1} and span exactly the same range that rhodopin glucoside (12 400 cm^{-1}) and spheroidene (13 160 cm^{-1}), which are present in LH2.[25] A similar scenario is also observed for their $S_2(1^1B_u^+)$ energies. Undeniably, in this case, not $S_1(2^1A_g^-)$ and $S_2(1^1B_u^+)$ energies but overly large intermolecular distance is responsible for the lack of Car radical cation formation. This means that the Car molecules in the LHRC from *R. castenholzii* are not as closely packed to the BChls as they are in LH2 from purple bacteria. This suggestion is corroborated by the measured low energy transfer efficiencies.

4. Conclusions

The use of ultrafast TA spectroscopy in combination with steady-state fluorescence and absorption spectroscopy of LHRC complexes from *R. castenholzii* has revealed the identities and roles in energy transfer of bound Cars. TA spectroscopy of the purified Cars in solution allowed the determination of the $S_1(2^1A_g^-)$ energies. The results of global fitting of TA data sets coupled with single wavelength fitting of LHRC TA and fluorescence excitation measurements permitted the prediction of the Car-to-BChl energy transfer pathway. All the Cars present in LHRC complexes from *R. castenholzii* (except methoxy-keto-myxocoxanthin) have similar excited states energies ($S_1(2^1A_g^-)$ and $S_2(1^1B_u^+)$) to spheroidene, the carotenoid present in LH2 complex from *Rb. sphaeroides*. By analogy they should be very well tuned to carry out efficient energy transfer to BChls (energy transfer efficiency of spheroidene in the LH2 complex is >90%[25]). However, the lack of Car radical cation formation in the present complexes suggests a significantly larger Car−BChl intermolecular distance than present in the LH2 complex. Despite the spectral similarity between the LHRC from *R. castenholzii* and the LH2 complex from purple bacteria, the Car−BChl distance is expected to be larger in this complex and is very probably the major reason for the low Car-to-BChl energy transfer efficiency observed here.

Acknowledgment. This research is from the Photosynthetic Antenna Research Center (PARC), an Energy Frontier Research Center funded by the DOE, Office of Science, Office of Basic Energy Sciences under Award Number DE-SC 0001035. This work was also supported by DOE Grant DEFG02-07ER15846 to R.E.B. Work in the laboratory of HAF was supported by grants from the National Science Foundation (MCB-0913022) and the University of Connecticut Research Foundation.

Supporting Information Available: Comparison of HPLC chromatograms of nonsaponified and saponified pigment extract of the anaerobic and the aerobic LHRC complexes, HPLC chromatograms of saponified and then $NaBH_4$-reduced pigment extract from the aerobic LHRC complex, mass spectroscopy results, the LH-only absorption spectra of the anaerobic and the aerobic complexes obtained by subtracting the absorption spectrum of RC, goodness of the spectral reconstruction of the Car band of LH-only absorption spectra tested by subtracting the fit from the raw spectrum, the kinetics extracted at the maximum, blue and red sides of the major VIS TA band and in range of the $S_2(1^1B_u^+) \rightarrow S_n$ and the $S_1(2^1A_g^-) \rightarrow S_2$ transitions (NIR) with accompanied fits, TA and global fitting results of keto-γ-carotene and methoxy-keto-myxocoxanthin in methanol, detailed information about fits from Figure 12. This material is available free of charge via the Internet at http://pubs.acs.org.

References and Notes

(1) Hudson, B.; Kohler, B. *Annu. Rev. Phys. Chem.* **1974**, *25*, 437.
(2) Hudson, B. S.; Kohler, B. E.; Schulten, K. Linear Polyene Electronic Structure and Potential Surfaces. In *Excited States*; Lim, E. D., Ed.; Academic Press: New York, 1982; p 1.
(3) Schulten, K.; Karplus, M. *Chem. Phys. Lett.* **1972**, *14*, 305.
(4) Tavan, P.; Schulten, K. *J. Chem. Phys.* **1979**, *70*, 5407.
(5) Tavan, P.; Schulten, K. *Phys. Rev. B: Condens. Matter* **1987**, *36* (8), 4337.
(6) Hanada, S.; Takaichi, S.; Matsuura, K.; Nakamura, K. *Int. J. Syst. Evol. Microbiol.* **2002**, *52*, 187.
(7) Hanada, S. *Microbes Environ.* **2003**, *18* (2), 51.
(8) Collins, A. M.; Xin, Y. Y.; Blankenship, R. E. *Biochim. Biophys. Acta, Bioenerg.* **2009**, *1787* (8), 1050.
(9) Takaichi, S.; Maoka, T.; Yamada, M.; Matsuura, K.; Haikawa, Y.; Hanada, S. *Plant Cell Physiol.* **2001**, *42* (12), 1355.
(10) Takaichi, S. *Photosynth. Res.* **2000**, *65* (1), 93.
(11) Takaichi, S.; Ishidsu, J. *Methods Enzymol.* **1992**, *213*, 366.
(12) Ilagan, R. P.; Christensen, R. L.; Chapp, T. W.; Gibson, G. N.; Pascher, T.; Polivka, T.; Frank, H. A. *J. Phys. Chem. A* **2005**, *109* (14), 3120.
(13) Niedzwiedzki, D. M.; Sullivan, J. O.; Polivka, T.; Birge, R. R.; Frank, H. A. *J. Phys. Chem. B* **2006**, *110* (45), 22872.
(14) Pendon, Z. D.; Sullivan, J. O.; van der Hoef, I.; Lugtenburg, J.; Cua, A.; Bocian, D. F.; Birge, R. R.; Frank, H. A. *Photosynth. Res.* **2005**, *86* (1−2), 5.
(15) Niedzwiedzki, D.; Cong, H.; Sullivan, J. O.; Gibson, G. N.; Birge, R. R.; Frank, H. A. *J. Phys. Chem. B* **2007**, *111* (21), 5984.
(16) Billsten, H. H.; Bhosale, P.; Yemelyanov, A.; Bernstein, P. S.; Polivka, T. *Photochem. Photobiol.* **2003**, *78* (2), 138.
(17) Billsten, H. H.; Pan, J.; Sinha, S.; Pascher, T.; Sundstrom, V.; Polivka, T. *J. Phys. Chem. A* **2005**, *109* (31), 6852.
(18) Wohlleben, W.; Buckup, T.; Herek, J. L.; Cogdell, R. J.; Motzkus, M. *Biophys. J.* **2003**, *85* (1), 442.
(19) Wohlleben, W.; Buckup, T.; Hashimoto, H.; Cogdell, R. J.; Herek, J. L.; Motzkus, M. *J. Phys. Chem. B* **2004**, *108* (10), 3320.
(20) Niedzwiedzki, D. M.; Cong, H.; Sandberg, M. N.; Gibson, G. N.; Birge, R. R.; Frank, H. A. *Chem. Phys.* **2009**, *357* (1−3), 4.
(21) Larsen, D. S.; van Stokkum, I. H. M.; Vengris, M.; Kennis, J. T. M.; van Grondelle, R. *Chem. Phys. Lett.* **2003**, *381* (5−6), 733.
(22) Papagiannakis, E.; van Stokkum, I. H.; Vengris, M.; Cogdell, R. J.; van Grondelle, R.; Larsen, D. S. *J. Phys. Chem. B* **2006**, *110* (11), 5727.
(23) Zhang, J. P.; Fujii, R.; Koyama, Y.; Rondonuwu, F. S.; Watanabe, Y.; Mortensen, A.; Skibsted, L. H. *Chem. Phys. Lett.* **2001**, *348* (3−4), 235.
(24) Polivka, T.; Zigmantas, D.; Frank, H. A.; Bautista, J. A.; Herek, J. L.; Koyama, Y.; Fujii, R.; Sundstrom, V. *J. Phys. Chem. B* **2001**, *105* (5), 1072.
(25) Cong, H.; Niedzwiedzki, D. M.; Gibson, G. N.; LaFountain, A. M.; Kelsh, R. M.; Gardiner, A. T.; Cogdell, R. J.; Frank, H. A. *J. Phys. Chem. B* **2008**, *112* (34), 10689.
(26) Niedzwiedzki, D. M.; Chatterjee, N.; Enriquez, M. M.; Kajikawa, T.; Hasegawa, S.; Katsumura, S.; Frank, H. A. *J. Phys. Chem. B* **2009**, *113* (41), 13604.
(27) Shima, S.; Ilagan, R. P.; Gillespie, N.; Sommer, B. J.; Hiller, R. G.; Sharples, F. P.; Frank, H. A.; Birge, R. R. *J. Phys. Chem. A* **2003**, *107* (40), 8052.
(28) van Stokkum, I. H.; Larsen, D. S.; van Grondelle, R. *Biochim. Biophys. Acta* **2004**, *1657* (2−3), 82.
(29) Fujii, R.; Inaba, T.; Watanabe, Y.; Koyama, Y.; Zhang, J. P. *Chem. Phys. Lett.* **2003**, *369* (1−2), 165.
(30) Billsten, H. H.; Zigmantas, D.; Sundstrom, V.; Polivka, T. *Chem. Phys. Lett.* **2002**, *355* (5−6), 465.
(31) Gradinaru, C. C.; Kennis, J. T.; Papagiannakis, E.; van Stokkum, I. H.; Cogdell, R. J.; Fleming, G. R.; Niederman, R. A.; van Grondelle, R. *Proc. Natl. Acad. Sci. U. S. A.* **2001**, *98* (5), 2364.
(32) Chynwat, V.; Frank, H. A. *Chem. Phys.* **1995**, *194* (2−3), 237.
(33) Englman, R.; Jortner, J. *J Mol Phys* **1970**, *18*, p. 145.
(34) Förster, T. Action of Light and Organic Crystals. In *Modern Quantum Chemistry*; Sinanoglu, O. Ed.; Academic Press: New York, 1965; Vol. 3.
(35) Scholes, G. D.; Harcourt, R. D.; Fleming, G. R. *J. Phys. Chem. B* **1997**, *1997* (101), 7302.
(36) Zigmantas, D.; Polivka, T.; Hiller, R. G.; Yartsev, A.; Sundstrom, V. *J. Phys. Chem. A* **2001**, *105* (45), 10296.
(37) Frank, H. A.; Bautista, J. A.; Josue, J.; Pendon, Z.; Hiller, R. G.; Sharples, F. P.; Gosztola, D.; Wasielewski, M. R. *J. Phys. Chem. B* **2000**, *104* (18), 4569.
(38) Papagiannakis, E.; Kennis, J. T.; van Stokkum, I. H.; Cogdell, R. J.; van Grondelle, R. *Proc. Natl. Acad. Sci. U. S. A.* **2002**, *99* (9), 6017.
(39) Hashimoto, H.; Koyama, Y.; Hirata, Y.; Mataga, N. *J. Phys. Chem.-Us* **1991**, *95* (8), 3072.
(40) Rondonuwu, F. S.; Watanabe, Y.; Fujii, R.; Koyama, Y. *Chem. Phys. Lett.* **2003**, *376* (3−4), 292.
(41) Polivka, T.; Pullerits, T.; Frank, H. A.; Cogdell, R. J.; Sundstrom, V. *J. Phys. Chem. B* **2004**, *108* (39), 15398.
(42) Chadwick, B. W.; Zhang, C. Y.; Cogdell, R. J.; Frank, H. A. *Biochim. Biophys. Acta* **1987**, *893* (3), 444.
(43) Wormit, M.; Dreuw, A. *J. Phys. Chem. B* **2006**, *110* (47), 24200.
(44) Mcdermott, G.; Prince, S. M.; Freer, A. A.; Hawthornthwaitelawless, A. M.; Papiz, M. Z.; Cogdell, R. J.; Isaacs, N. W. *Nature* **1995**, *374* (6522), 517.
(45) Montano, G. A.; Xin, Y. Y.; Lin, S.; Blankenship, R. E. *J. Phys. Chem. B* **2004**, *108* (29), 10607.

JP1005764